MP2, density functional theory, and molecular mechanical calculations of C–H···π and hydrogen bond interactions in a cellulose-binding module–cellulose model system

ARTICLE *in* CARBOHYDRATE RESEARCH · AUGUST 2010

Impact Factor: 1.93 · DOI: 10.1016/j.carres.2010.05.021 · Source: PubMed

5 AUTHORS, INCLUDING:

Mohamed Naseer ali Mohamed
The New College
15 PUBLICATIONS **149** CITATIONS
SEE PROFILE

Heath Watts
Pennsylvania State University
14 PUBLICATIONS **98** CITATIONS
SEE PROFILE

Jing Guo
University of Denver
91 PUBLICATIONS **1,341** CITATIONS
SEE PROFILE

J. D. Kubicki
University of Texas at El Paso
216 PUBLICATIONS **4,438** CITATIONS
SEE PROFILE

Carbohydrate Research 345 (2010) 1741–1751

Contents lists available at ScienceDirect

Carbohydrate Research

journal homepage: www.elsevier.com/locate/carres

MP2, density functional theory, and molecular mechanical calculations of C–H···π and hydrogen bond interactions in a cellulose-binding module–cellulose model system

Mohamed Naseer Ali Mohamed [a,d], Heath D. Watts [a,d], Jing Guo [b,d], Jeffrey M. Catchmark [c,d], James D. Kubicki [a,d,*]

[a] Department of Geosciences and the Earth & Environmental Systems Institute, The Pennsylvania State University, University Park, PA 16802, USA
[b] Department of Plant Biology, The Pennsylvania State University, University Park, PA 16802, USA
[c] Department of Agricultural and Biological Engineering, The Pennsylvania State University, University Park, PA 16802, USA
[d] Center for NanoCellulosics, The Pennsylvania State University, University Park, PA 16802, USA

ARTICLE INFO

Article history:
Received 19 April 2010
Received in revised form 10 May 2010
Accepted 22 May 2010
Available online 8 June 2010

Keywords:
C–H···π interaction
Carbohydrate-binding module
Cellulose
Quantum Mechanical

ABSTRACT

Exploring non-covalent interactions, such as C–H···π stacking and classical hydrogen bonding (H-bonding), between carbohydrates and carbohydrate-binding modules (CBMs) is an important task in glycobiology. The present study focuses on intermolecular interactions, such as C–H···π (sugar–aromatic stacking) and H-bonds, between methyl β-D-glucopyranoside and L-tyrosine—a proxy model system for a cellulose–CBM complex. This work has made use of various types of quantum mechanics (QM) and molecular mechanics (MM) methods to determine which is the most accurate and computationally efficient. The calculated interaction potential energies ranged between −24 and −38 kJ/mol. The larger interaction energy is due to H-bonding between the phenyl hydroxyl of tyrosine and the O4 of the sugar. Density functional theory (DFT) methods, such as BHandHLYP and B3LYP, exaggerate the H-bond. Although one of the MM methods (viz. MM+) considered in this study does maintain the C–H···π stacking configuration, it underestimates the interaction energy due to the loss of the H-bond. When the O–H bond vector is in the vicinity of O4 (O–H···O4 ≈ 2 Å, e.g., in the case of MP2/6-31G(d)), the torsional energy drops to a minimum. For this configuration, natural bond orbital (NBO) analysis also supports the presence of this H-bond which arises due to orbital interaction between one lone pair of the sugar O4 and the σ^*(O–H) orbital of the phenyl group of tyrosine. The stabilization energy due to orbital delocalization of the H-bonded system is ∼13 kJ/mol. This H-bond interaction plays an important role in controlling the CH/π interaction geometry. Therefore, the C–H···π dispersive interaction is the secondary force, which supports the stabilization of the complex. The meta-hybrid DFT method, M05-2X, with the 6-311++G(d,p) basis set agrees well with the MP2 results and is less computationally expensive. However, the M05-2X method is strongly basis set dependent in describing this CH/π interaction. Computed IR spectra with the MP2/6-31G(d) method show blue shifts for C1–H, C3–H, and C5–H stretching frequencies due to the C–H···π interaction. However, the M05-2X/6-311++G(d,p) method shows a small red shift for the C1–H stretching region and blue shifts for the C2–H and C3–H stretches. For the aromatic tyrosine $C_{\delta1}$–$C_{\varepsilon1}$ and $C_{\delta2}$–$C_{\varepsilon2}$ bonds in the complex, the calculated IR spectra show red shifts of 12 cm^{-1} (MP2/6-31G(d)) and 5 cm^{-1} (M05-2X/6-311++G(d,p)). This study also reports the upfield shifts of computed ^{1}H NMR chemical shifts due to the C–H···π interaction.

1. Introduction

Cellulose degradation processes in nature are governed by the action of several types of cellulolytic enzymes. Most of the fungal cellulases have a bifunctional organization in which a catalytic core domain and a cellulose-binding module (CBM) are connected through a flexible linker peptide.[1,2] Though both domains are present close to the cellulose surface, the affinity of the CBM is thought to be the predominant one over the catalytic domain. Hence, the binding of cellulose is mediated by the CBM and is necessary for an efficient attack of cellulose by the enzyme before degradation can take place.[3]

CBM family classifications are based on the amino acid sequence similarity (see http://www.cazy.org).[4] These families have been grouped manually as functional types into 'Type A' (e.g., families 1, 2a, 3–5, and 10) 'Type B' (e.g., families 4, 15, and 17), and 'Type C' (e.g., families 9, 13, 14, 18, and 32) from the available crys-

* Corresponding author.
E-mail address: jdk7@psu.edu (J.D. Kubicki).

0008-6215/$ - see front matter © 2010 Elsevier Ltd. All rights reserved.
doi:10.1016/j.carres.2010.05.021

tal structures.[5] CBMs that are specific for insoluble cellulose can be grouped into two general categories: those that interact with crystalline cellulose (Type A) and those that interact with non-crystalline cellulose (Type B). These functional groupings pertain to both fungal and bacterial CBMs. The binding site topography of Type A is characterized by a planar surface such that the planar hydrophobic face of the crystalline cellulose surface interacts favorably. The valley-shaped Type B CBMs are suitable for binding individual glycan chains. These topographies can be utilized in biotechnological applications such as designing molecular linkers for cellulose. In the CBM of cellulase/hemicellulase and other carbohydrate-binding proteins, the side chains of these aromatic residues provide a hydrophobic platform through stacking interactions to mediate the sugar recognition.[6] This hydrophobic platform can be a planar, twisted, or sandwich structure depending on the type of CBMs.[5] From the reported amino acid sequences of several fungal, the CBMs of Type A show strong sequence similarity. Among them, the conserved residues; tyrosine, tryptophan, and phenylalanine are involved directly in the cellulose recognition process.[3]

Mutational studies also revealed that adjacent conserved residues of these aromatic amino acids in the CBM do not show any direct H-bonds with the crystalline cellulose.[7] However, CBMs do H-bond in the case of adsorption to non-crystalline cellulose.[8] Thus, these studies indicate that H-bonding and C–H···π, hydrophobic driving forces are involved in cellulose recognition by the CBM. Recently, there are studies showing that a dispersive interaction is a driving force for the specificity and affinity of the CBMs to crystalline cellulose.[5] These interactions are mediated by the stacking of aromatic residues of CBM binding site with apolar patches formed by the sugar H-atoms of the cellulose. Binding of these proteins mediates the recognition process and initiates the defibrillation process, by disturbing inter- and intramolecular H-bonds of the cellulose fiber.[9] Therefore, knowledge of the possible interactions between CBMs and cellulose at the atomic and electronic levels is an important step in the task of designing cellulose linkers and for understanding cellulose degradation. Toward this end, efforts have been made to understand the molecular-level interactions that cause sugar recognition through these residues using quantum mechanical (QM) and molecular mechanical (MM) investigations.

Stacking between carbohydrates and aromatic side chains occurs in the CBM as well as the catalytic region of cellulolytic enzymes and other sugar-binding proteins. Stacking between carbohydrates and side chains of aromatic amino acids in CBMs (e.g., tyrosine) is due to the interaction between the π-orbitals of aromatic carbons and the C–H groups of the hydrophobic regions of sugars. This stacking interaction is thought to be a hydrophobic–hydrophobic interaction.[10–12] Recently, this stacking, dispersive or van der Waals interaction has been identified as a 'C–H···π' interaction or bond and it is much weaker than classical H-bonds (i.e., <4 kJ/mol compared to 10–40 kJ/mol).[13]

Earlier computational studies of the structure and energetics of non-carbohydrate C–H···π interacting systems, at various levels of theory, suggested the importance of electron correlation terms to identify the presence of this dispersion force.[14–16] Therefore, accurate calculation of intermolecular electron correlation is critical to model these interactions. In addition, these computational approaches and the Cambridge Structural Database (CSD) analyses explore the nature of the configurations of the donor C–H group with reference to the acceptor aromatic ring.[17] Hence, these approaches pointed out the directionality of the C–H bond vector in determining the strength of the C–H···π interaction. The results of these studies indicated that the highly populated and most stable configuration is the one wherein the C–H bond should be positioned at the center of the aromatic ring (−6 kJ/mol). Energetics of these studies in the case of benzene–methane complex also suggested two other possible configurations in that the C–H bond vector is perpendicular to the aromatic bond center (interaction energy of −2 kJ/mol) or aromatic carbon (−2 kJ/mol). Also, the energetics of C_6H_6–C_2H_6, C_6H_6–C_2H_4 and C_6H_6–C_2H_2 complexes indicating that the positioning of H atom in the donor C–H group should lie perpendicular to the center of the ring and not the C atom. These studies provide guidance toward building models for analyzing the C–H···π interactions in cellulose–CBM complexes.

For this work, methyl β-D-glucopyranoside (OMG) and L-tyrosine (Tyr) were used as model proxies for cellulose and a CBM, respectively (Fig. 1). In OMG, the hydrophobic face contains three C–H groups (viz. C1–H1, C3–H3, and C5–H5), which are aligned perpendicular to the aromatic plane, so that each C–H group interacts with a different aromatic carbon. Because the C–H···π interactions are additive, there are three different C–H···π interactions possible. In addition, one H-bond can form between the phenyl hydroxyl of Tyr and one of the sugar hydroxyls (Fig. 1). Earlier studies on related systems with C–H···π configurations showed that the interaction energies varied from −2 to −27 kJ/mol for complexes lacking H-bonds, to a maximum of −51 kJ/mol for the H-bonded ($O–H_{phenyl}\cdots O_{glc}$) glucose–aromatic complex systems.[18,19]

As the sugar hydroxyls (viz. 2,3,6 hydroxyls) are strongly H-bonded with their neighboring sugars in the cellulose crystal,[20] energy would be required for them to change their orientation in order to form H-bonds with the side chains (phenyl hydroxyls) of tyrosine when the CBM anchors the cellulose surface. Either the phenyl hydroxyl orients itself trans to the plane of the phenyl ring to form a H-bond with the sugar acceptor or cis to the plane to form H-bond with water. The hindrance to phenyl O–H bond rotation is caused by the energy barrier when the σ_{OH} orbitals interact unfavorably with the π-orbitals of the aromatic carbons. This work will determine if the Tyr O–H bond rotation barrier can be overcome by H-bonding with OMG hydroxyl groups. To evaluate this hypothesis, the orbital distribution in the isolated Tyr and the OMG–Tyr complex were calculated.

NMR is a valuable tool for studying the structural features and inter- and intramolecular interactions in carbohydrates.[21–23] ^{1}H NMR techniques have been used widely in characterizing the weak C–H···π-type interactions in small molecular systems. Recent studies using ^{1}H NMR to characterize C–H···π interactions

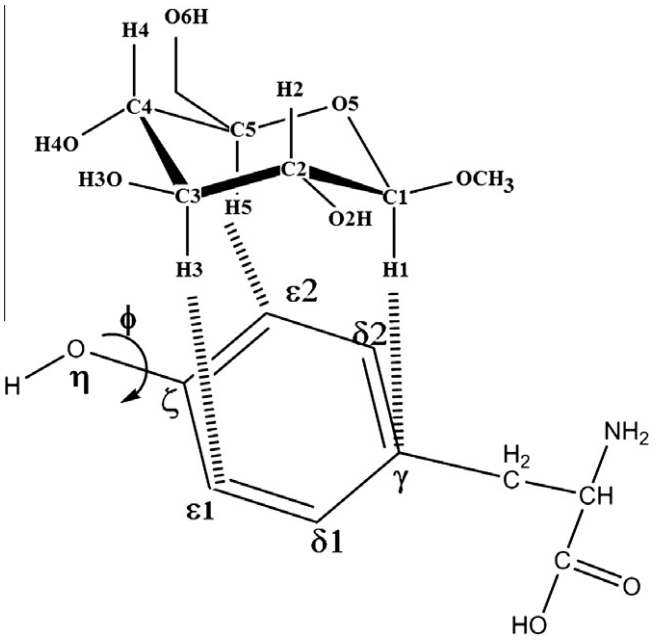

Figure 1. Numbering scheme of the dimer model. Torsional definition of phenol hydroxyl rotation is $\phi = \phi$ (Cε–Cζ–Oη–H).

between sugars and aromatic molecules show the importance of π electrons of aromatic systems in mediating the sugar specificity.[18,24] The chemical shifts of the apolar protons have been shown to be modified according to their spatial positions in the field created by the aromatic ring current. As no report was found for the beta anomeric sugar with tyrosine, the present study will compute the shielding of the protons in the beta anomeric form of glucose in a stacked configuration with tyrosine. Observed experimental chemical shifts on related systems available from the literature will be compared with the computed ^{1}H NMR chemical shifts.

2. Results and discussion

2.1. Interaction energies and geometries

Complete energy minimizations of the CBM–cellulose model viz. OMG–Tyr complex were performed with the BHandHLYP/cc-pVTZ and MP2/6-31G(d,p) methods and the corresponding optimized structures are shown in Figure 2. The starting geometry of the model was the same for both calculations. Although BHandHLYP has been proposed as a viable alternative to the MPn methods for calculating the C–H···π interactions in small model peptides found in hydrophobic core of certain proteins,[25–27] the optimized structure reveals that the BHandHLYP/cc-pVTZ method does not describe the C–H···π interaction in the case of OMG–Tyr because the stacking of the sugar and phenyl ring does not occur (Fig. 2b). The interaction between monomers as predicted by the BHandHLYP/cc-pVTZ method is dominated instead by H-bonding.

The size of the model under investigation is reasonably a large one to perform a flexible scan of intermolecular potential energy surface using the MP2/6-31G(d,p) method. The MP2/6-31G(d) optimization of the model provides similar structural parameters (C–H1···C = 2.95 Å, C–H3···C = 2.61 Å, C–H5···C = 2.47 Å) compared to experimental values[28,29] (Table 1). Therefore, further computations were carried out using MP2/6-31G(d) geometry. The minimum-energy structures obtained at this level were also used to produce a potential energy surface (PES) with single-point calculations with a larger basis set viz. MP2/6-311+G(d,p)//MP2/6-31G(d).

The PES of optimized OMG–Tyr complex was analyzed by individually varying the distance between (i) the C1 of sugar and Cγ of the phenyl ring (describes the inter-ring separation) and (ii) the H1 of the sugar and Cγ of the phenyl ring. These two different approaches in PES scan were used to study the CH/π interactions in the related systems by various authors.[16,19] In the present study, these two scans were done together to test which is the more appropriate one than the other. The C1···Cγ and H1···Cγ scan were carried out by varying the non-bonded distances starting from 2.9 to 4.4 Å and from 2 to 3.4 Å, respectively, with a step size of 0.1 Å. All other atomic coordinates were allowed to relax. The obtained C1···Cγ and C1–H1···Cγ non-bonded potential energy curves are shown in Figure 3a and b and their interaction energy profiles as a function of distance are shown in Figure 3c and d. The potential energy curve describes the nature of interaction potential by these hydrophobic groups. On comparison of the Figure 3a and b, it is seen that a local minimum appears in the case of C1···Cγ scan at C1···Cγ = 3.1 Å. At this configuration of the complex, H1 of the C1 slightly moved out of Cγ and pointing inside the aromatic ring due to electronic repulsion experienced by it. This causes the tilting of sugar ring plane from the aromatic ring plane thereby acquiring a O–H···π interaction through phenol aromatic carbon and O2 of sugar hydroxyl hence stabilizing the complex at this configuration (Fig. S3). However, we believe that the appeared local minimum is not a significant one as the non-covalent distance between H1 and Cγ is short. Therefore, from two different scanning performed, we are suggesting that the C···H scan would be more appropriate one than the C···C scan in studying the C–H···π interactions in sugar-aromatic complexes.

From Figure 3, the interaction potentials are weak as a function of distance evidenced by the shallow minimum energy region in both cases. For example, the potential energy of the complex varies by <5 kJ/mol over a range of 2.5–3.2 Å. The computed C1–H1···C(γ) and C1···C(γ) non-bonded minima are found to occur at 3.0 and 4.2 Å with the MP2/6-31G(d) basis set. Frequency calculations at MP2/6-31G(d) level confirmed that the obtained structure was a minimum on the PES, because all of the calculated frequencies were positive. (Note: This does not imply that other minima do not exist and that this is the global potential energy minimum for this system.) Using the MP2/6-311+G(d,p)//MP2/6-31G(d) po-

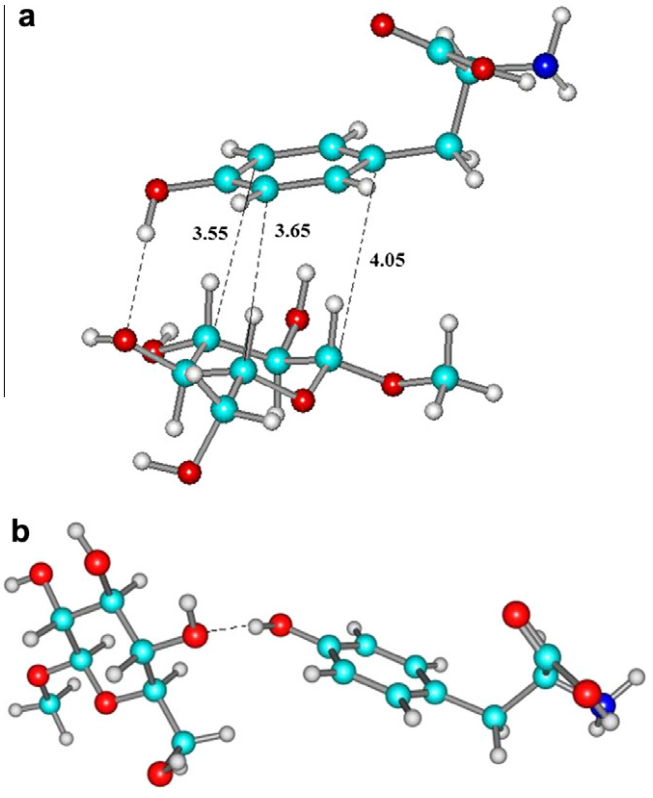

Figure 2. Minimized structure of Glc-Tyr dimer model (a) MP2/6-31G(d,p) and (b) BHandHLYP/ccpVTZ—HyperChem has been used for ball and stick rendering of the model.

Table 1
The experimental interaction distance geometry matrixes were obtained from the RCSB Protein Data Bank[28] in combination with the tool *GlyVicinity[29]

Tyr	Glc[a]						
	C1	C2	C3	C5	H1	H3	H5
C			3.90(1)				
CA	3.77(4)	3.66(5)	—	3.93(3)			
CB	4.00(3)	3.90(4)	3.66(5)	3.87(13)			
CD1	3.80(11)	3.66(28)	3.78(23)	3.77(22)			3.0(1)
CD2	3.86(12)	3.91(12)	3.90(5)	3.87(26)	3.1(1)	3.2(1)	
CE1	3.81(27)	3.79(35)	3.76(17)	3.84(31)	3.1(1)	3.9(1)	
CE2	3.74(27)	3.78(26)	3.82(12)	3.78(41)	3.0(1)	3.0(1)	
CG	3.73(3)	3.71(8)	4.0(3)	3.81(30)			2.8(1)
CZ	3.82(24)	3.79(29)	3.82(18)	3.81(44)	3.0(1)		2.7(1)

The tyrosine residues were selected within 4 Å radius of β-D-Glc in protein complex solved within 3.5 Å resolution.

[a] Values in parenthesis represent the number of occurrences.

* http://www.glycosciences.de/index.php.

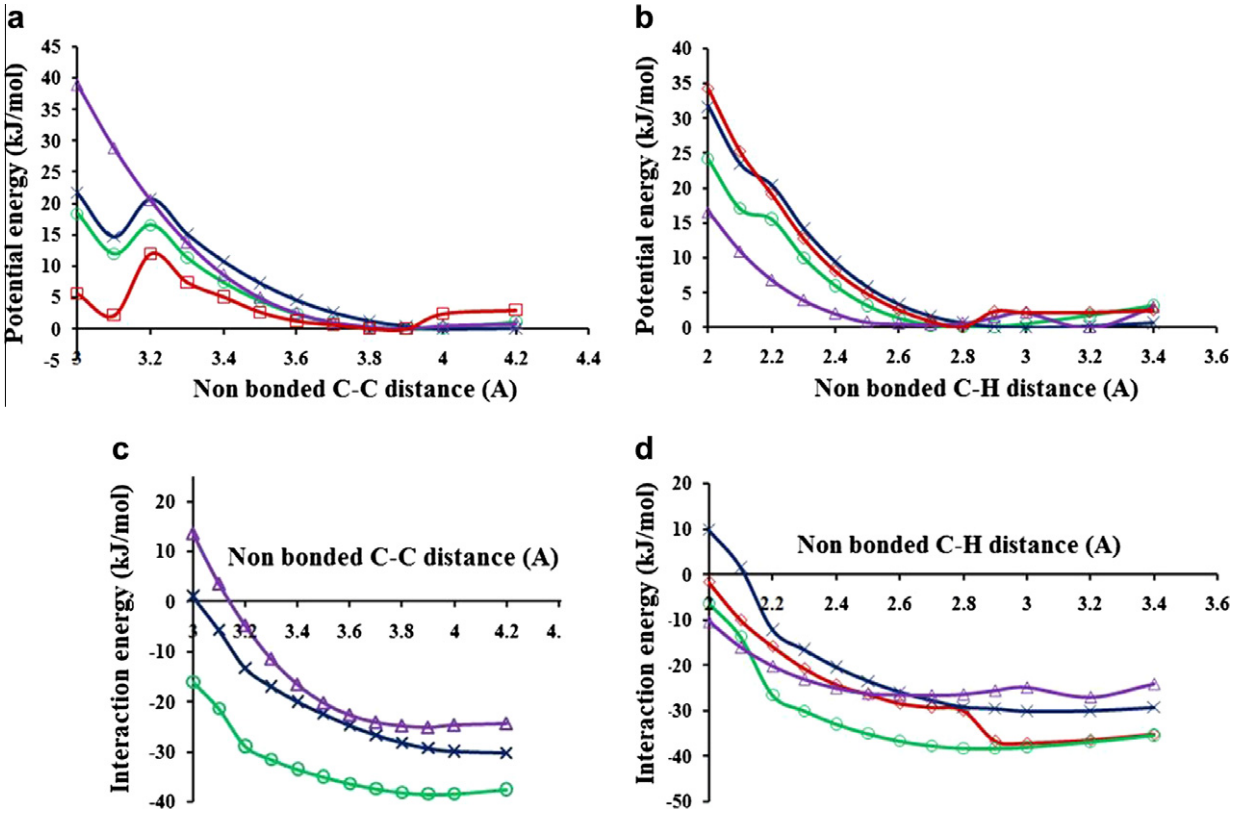

Figure 3. Variation of potential energy as a function of C1···Cγ (a) and CH1···Cγ (b) distances. Corresponding variation of interaction energies (c and d) have also been depicted. The adapted computational methods are MM+ (), MP2/6-31G(d) (), MP2/6-311+G(d,p) (), and M05-2x/6-311+G(d,p) ().

tential energies, the C1–H1···C(γ) and C1···C(γ) non-bonded minima occur at 2.9 and 3.9 Å, respectively; thus the position of minimum is slightly different with a more accurate basis set using the same structures. In both cases, the predicted geometries fall within the distances reported for similar C–H···π systems (Table 1). There are no appreciable changes in the shapes of the PESs for the complex as the two molecules are separated farther from their minima (Fig. 3a and b).

Recent development of density functionals to model stacking interactions dominated by correlation energy (i.e., van der Waals forces) has resulted in the functional M05-2X.[30] To test the ability of this recently developed meta-hybrid density functional viz. M05-2X method to predict the C–H···π interactions for the present case, we have carried out benchmark calculations with various basis sets (Watts et al., unpublished results). These calculations show that M05-2X/6-311++G(d,p) energy minimization results in a reasonable approximation of the C–H···π stacking configuration of the OMG–Tyr complex, when compared with the results computed with MP2/6-31G(d) and MP2/6-311++G(d,p). Therefore, in this manuscript we have presented the interaction energy and geome-

Table 2
Computed interaction energies of the complex as a function of intermolecular distance using the QM and MM methods

Non-bonded [a] $C_{tyr}\cdots C_{glc}$ distance (Å)	ΔE_{int} (kJ/mol)				Non-bonded [b] $C_{tyr}\cdots H_{glc}$ distance (Å)	ΔE_{int} (kJ/mol)			
	MP2/6-31G(d)	MP2/6-311+G(d,p)//MP2/6-31G(d)	M05-2X/6-311++G(d,p)	MM+		MP2/6-31G(d)	MP2/6-311+G(d,p)//Mp2/6-31G(d)	M05-2X/6-311++G(d,p)	MM+
3.0	1.12	−15.99	−14.47	13.73	2	9.80	−6.40	−1.68	−10.32
3.1	−5.58	−21.36	−17.88	3.62	2.1	1.66	−13.71	−10.00	−15.97
3.2	−13.17	−28.80	−23.37	−4.70	2.2	−12.09	−26.48	−15.78	−20.11
3.3	−16.88	−31.45	−26.35	−11.43	2.3	−16.54	−30.00	−20.67	−23.00
3.4	−19.91	−33.43	−27.51	−16.56	2.4	−20.36	−32.87	−24.20	−24.93
3.5	−22.40	−34.93	−29.01	−20.24	2.5	−23.40	−35.03	−26.34	−26.14
3.6	−24.68	−36.29	−29.84	−22.69	2.6	−25.85	−36.63	−28.32	−26.39
3.7	−26.59	−37.31	−29.84	−24.15	2.7	−27.68	−37.67	−29.25	−26.52
3.8	−28.14	−38.05	−30.04	−24.85	2.8	−29.17	−38.21	−29.89	−26.31
3.9	−29.27	−38.42	−29.96	−25.19	2.9	−29.53	−38.26	−36.58	−25.47
4.0	−29.85	−38.32	−36.78	−24.71	3.0	−30.10	−37.97	−37.06	−24.80
4.2	−30.16	−37.46	−37.79	−24.64	3.2	−30.01	−36.81	−36.37	−26.93
					3.4	−29.29	−35.34	−35.15	−24.01

The interaction energy (ΔE) is computed using the sum of monomer energies obtained using the complex basis set.
[a] Distance between Cγ of L-tyrosine and C1 of methyl β-D-glucopyranoside (Fig. 1).
[b] Distance between Cγ of L-tyrosine and H1 of methyl β-D-glucopyranoside (Fig. 1).

try using the M05-2X method with 6-311++G(d,p) basis set and the results were compared with MP2 results (Table 2).

A relaxed potential energy scan was performed by varying the C–H non-bonded distance as was done in the previous case for the MP2 calculations. The variation of potential energies and the interaction energies as a function of non-bonded C–H distances are depicted in the Figure 3b and d. The results showed that the interaction energy is 1 kJ/mol less negative than that of MP2/6-311+G(d,p)//MP2/6-31G(d) and 7 kJ/mol more negative than MP2/6-31G(d). The interaction equilibrium C···H geometry has been found to be 3.0 Å which falls within the range predicted by these two quantum mechanical methods. However, this method underestimates the H-bonding O–H···O angle (140°) when compared to that from MP2 (158°) though the H-bond distance is the same (2.2 Å) for both methods. Verification that the structures were in a PES minimum was confirmed by frequency calculation at this level.

2.1.1. Comparison of force field results against MP2 method

The interaction energies obtained using MP2 and MM+ force field methods are shown in Figure 3. This figure indicates that the MM+ method follows the MP2 trends and the interaction energy is nearly 13 kJ/mol less negative when compared with MP2/6-311+G(d,p) method. The favorable interactions fall in the range of −25 to −38 kJ/mol in the order of MP2/6-311+G(d,p) > MP2/6-31G(d) > MM+. The present analysis of potential energies versus non-bonded C_{OMG}–CTyr distance shows that the MM+ and the MP2 methods have similar trends (Fig. 3a) except for the configurations corresponding to r_{C-C} = 3.1 and r_{C-H} = 2.1. At these configurations, the MP2/6-31G(d) models exhibit O–H···O-type H-bond (∼2.2 Å and 158° of H-bond geometry). These local minima were not found during energy minimizations with the MM+ force field method due to non-planarity of the O–H bond vector of the phenyl OH group at this configuration.

Correlations of the MM+ energies with MP2 energies are shown in Figure 4. The correlation coefficients are 0.98 for MP2/6-311+G(d,p) and 0.97 for MP2/6-31G(d). However, the MM+ method underestimates the interaction energies around the equilibrium configurations in comparison to MP2 results. The root-mean-squared-error between the MM+ force field calculation and the MP2 methods is 1.8 kJ/mol.

Test calculations using the other force field methods viz. MM2, AMBER, OPLS-AA (Fig. S1) reveal that the interaction energy is overestimated by MM2 and underestimated by the AMBER. The all-atom OPLS force field shows near equivalence to the MP2 interaction energy. Hence, these results indicate the ability of MM+ and OPLS-AA force fields to address the interactions due to C–H···π configuration of the investigating complex model. However, both the present and the earlier studies[19,31] clearly show the inaccuracy of these molecular mechanics force fields to account for the contribution of the H-bond interaction between phenyl hydroxyl and sugar hydroxyl onto the total interaction energy. To evaluate this claim, the contribution of the H-bond (between phenyl hydroxyl and sugar hydroxyl) energies to the total interaction energies was investigated; the obtained results are presented in the following section.

2.1.2. Phenyl hydroxyl rotation

In the case of cellulose-degrading enzymes, tyrosine residues interact with glucose (Glc) residues in crystalline cellulose. The stronger interaction energy predicted by the MP2 method, when compared to molecular mechanics, arises due to the existence of an H-bond between the phenyl hydroxyl of Tyr and a OMG hydroxyl. To estimate the contribution from this H-bond, a dihedral angle scan of the phenyl hydroxyl group was performed. For instance, when the phenyl hydroxyl group is in the plane of the phenyl ring

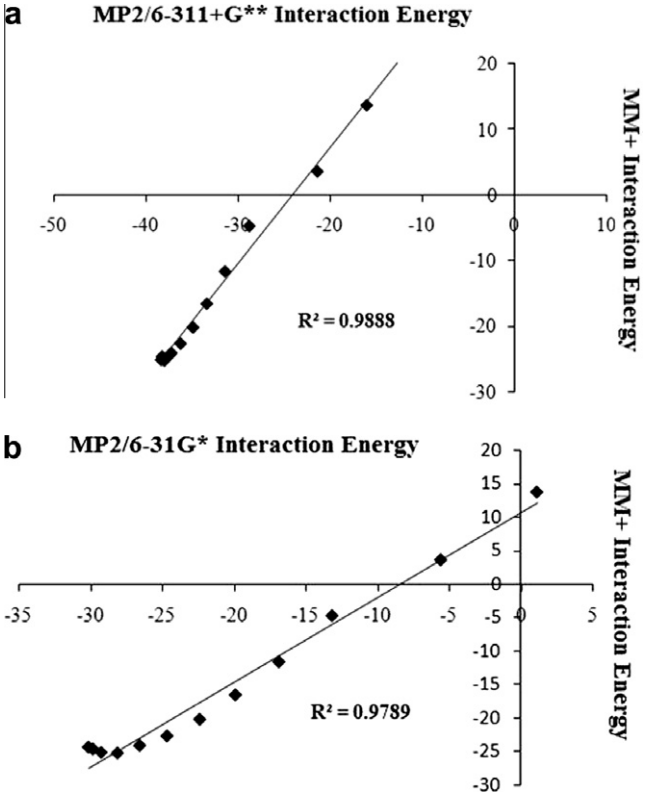

Figure 4. Correlation of MM+ interaction energies with that of (a) MP2/6-311+G(d,p)//MP2/6-31G(d) and (b) MP2/6-31G(d)//MP2/6-31G(d) interaction energies. The interaction energies are corresponding to C–C non-bonded distances.

(ϕ = 0°), there will be no H-bonding, and the energy difference between this configuration and the minimum energy configuration represents the energy contribution of the H-bond. The situation is more complex than this because strain energy within the tyrosine is generated by rotation of the hydroxyl group away from its preferred torsion angle for monomeric tyrosine (ϕ = −170°). The deconvolution of these two energy contributions (i.e., H-bonding and strain via rotation of the hydroxyl group) will be discussed below.

The obtained torsional profile is shown in Figure 5. From Figure 5a, it is evident that when the phenyl hydroxyl approaches the O4 atom of the sugar hydroxyl (ϕ = 140°), the energy drops to minimum, and when they move away from the O-4 sugar hydroxyl the energy increases. To separate the effects of the H-bond energy and the strain energy generated by changing the torsional angle on the overall energy of the complex, the same rotations of the hydroxyl group were performed for the isolated tyrosine (Fig. 5b) using the same methodology. Comparison of the tyrosine-only profile (Fig. 5b) with that of the complex (Fig. 5a) reveals that the global minimum for the complex occurs well below (by −28 kJ/mol) the one corresponding to isolated tyrosine (−7 kJ/mol Fig. 5b). Barriers occurred at ±90° in the isolated tyrosine (Fig. 5b) and at +60° and −90° in the Glc–Tyr complex (Fig. 5a). Although the planar configuration at ϕ = 0° of the tyrosine hydroxyl occurs in a relatively higher energy state, the transition to the deeper minimum should not be significantly hindered because of the low energy barrier (5–6 kJ/mol; Fig. 5a). This barrier is slightly higher (7–9 kJ/mol) in the case of isolated tyrosine (Fig. 5b) and indicates the ease transition of the conformational state in the presence of sugar hydroxyl.

An extensive study of protein–carbohydrate complexes obtained from six high-resolution (1.3 Å or better) X-ray structures

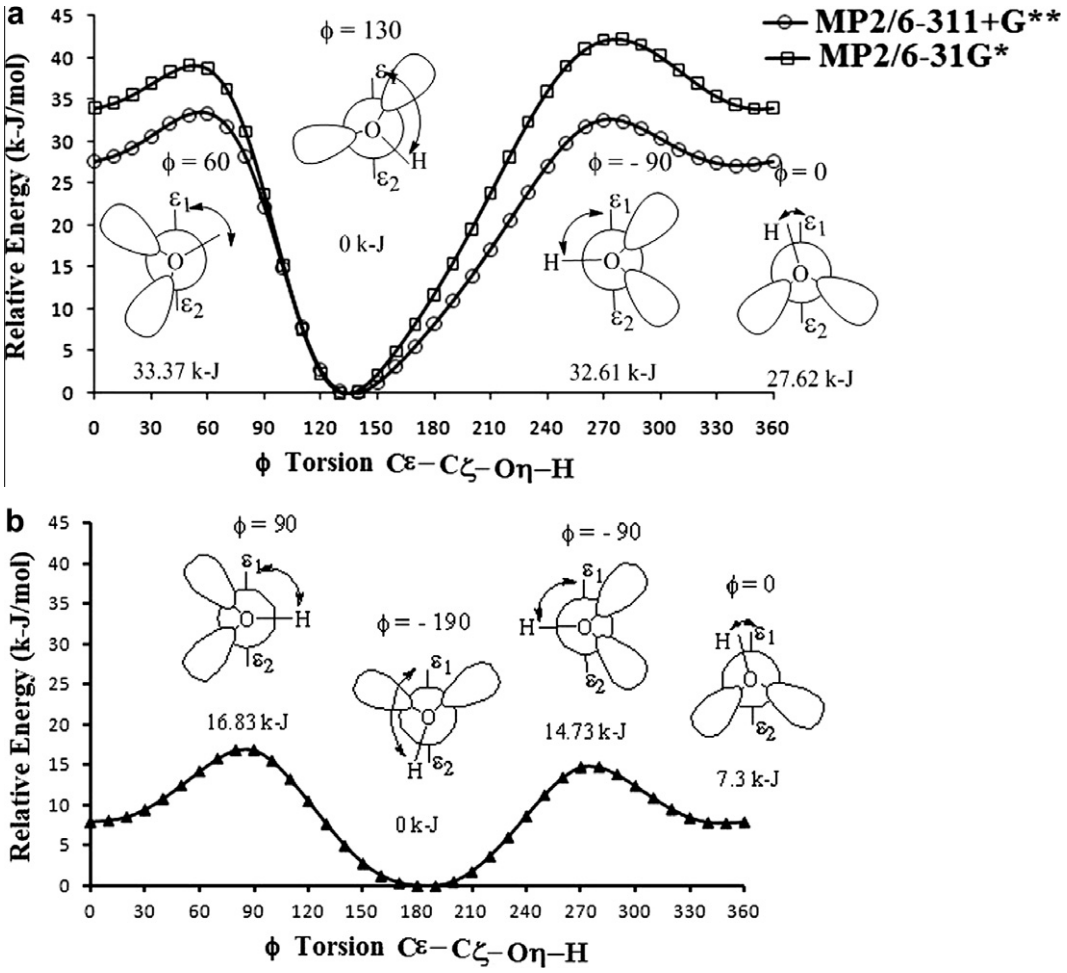

Figure 5. Variation of torsional energy as a function of ϕ for the (a) dimer and (b) tyrosine. Newman projection represents different configuration of phenol hydrogen.

has been undertaken by Spiwok et al.[19] Their studies indicate that the estimated interaction energies fall between −12 and −27 kJ/mol. They have also reported a large negative interaction energy value of about −51 kJ/mol, which is due to a classical H-bond as found for the present case. Hence, both Spiwok et al. study and our results show the existence of CH/π dispersive interactions together with H-bond.

The interaction energy predicted by MM calculations is found to be less favorable as it fails to show the presence of this H-bond. MM+ predicted the O4···H–O distance as 3.03 Å, and that the phenyl O–H group is co-planar with the phenyl ring (Fig. 6a). However, this configuration lies in the high-energy region of the MP2 PES. Hence, suggesting the necessity of optimization of these parameters to predict precisely both the C–H···π and H-bond interactions involved in the sugar recognition process by the aromatic amino acid-rich binding region of carbohydrate-binding proteins. Also, from these studies, none of these classical force field calculations predict the classical H-bond that exists between the hydroxyl group of Tyr and OMG O4 predicted via MP2 calculations (Fig. S2 and values in parentheses shown Fig. 6).

2.1.3. NBO analysis

NBO analysis is an effective tool for interpreting hyperconjugative interactions and electron density transfer.[32] Therefore, the stabilization of the OMG–Tyr complex by the intermolecular H-bond in conjunction with the CH/π interaction can be examined by analyzing the delocalization of the electron density and the cooperative effects of the $O4_{OMG} \rightarrow \sigma^*(O–H)_{Tyr,phenyl}$ and $\pi\,(C–C)_{phenyl} \rightarrow \sigma^*(C–H)_{sugar}$ orbital interactions using NBO analysis. The results of the NBO analysis are presented in Tables 3 and 4, and the highest occupied molecular orbitals (HOMOs) are shown in Figure 7. The intermolecular H-bond is formed by the orbital interaction between one lone pair of O4 of OMG and the σ^* (O–H) of the phenyl group of Tyr causing the stabilization of the H-bonded system with a stabilizing energy (E2) of about 13 kJ/mol (Table 3). Hence, the H-bond interaction leads to an increase in electron density of O–H anti-bonding orbital (75%, Table 4). In addition, the NBO analysis clearly shows the existence of the CH/π intermolecular interaction with the associated hyperconjugative interaction energies of about 5 and 2 kJ/mol, respectively (Table 3), which is due to the accumulation of electron density drawn from the $C–C_{phenyl}$ (Fig. 7) π-orbitals toward the C–H anti-bonding orbitals of OMG.

This charge delocalization is operative because of the respective distances 2.8, 2.6, and 2.5 Å between the interacting H in OMG and C_{sp2} in the aromatic ring. Bond distances such as C1–H1···C_{sp2}, C3–H3···C_{sp2}, and C5–H5···C_{sp2} are less than the sum of van der Waals radii (2.9 Å). The C3–H3···C and C5–H5···C contact distances are shorter than the C1–H1···C distance due to an attractive force exerted by the phenyl hydroxyl on O4 of OMG. To investigate this favorable O···H classical H-bond interaction on the torsional potentials of phenyl OH rotation, the non-bonded O···H distances were also calculated in the lowest *trans* (140°) and *gauche* (60° and −90°––the barriers) conformations of the phenyl OH group. For the trans conformation, the separation between the phenyl hy-

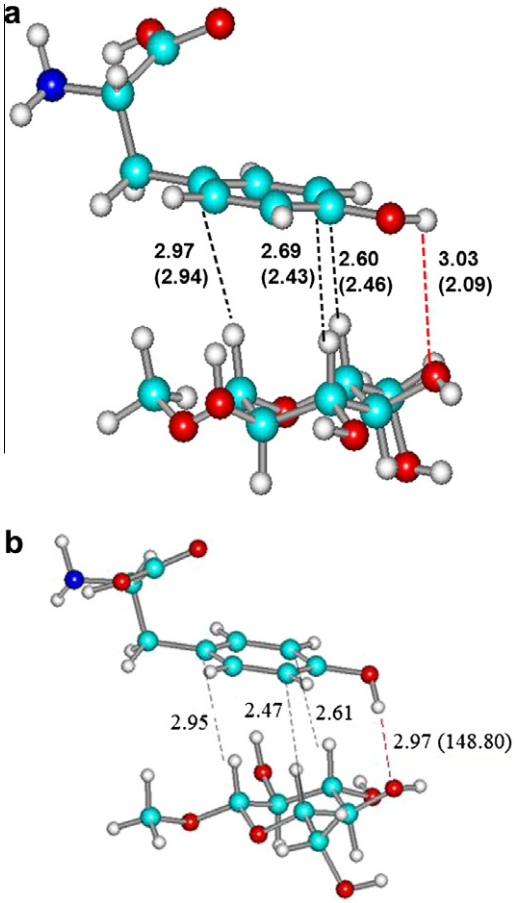

Figure 6. Optimized models of dimer (a) MM+ and the values in parenthesis correspond to ab initio one obtained using MP2/6-31G(d,p) level (b) MP2/6-31G(d). The H-bond has been shown in a red dashed line. (For interpretation of the references to color in this figure legend, the reader is referred to the web version of this article.)

Table 3
Interaction energies of the donor and acceptor orbitals showing the H-bond C–H···π interactions

Model	Phenyl hydroxyl rotation angle Π (°)	Donor NBO	Acceptor NBO	Stabilization energy E(2) (kJ/mol)
Complex	140*	[a]Cγ···Cδ2	[c]σ*C1–H1(**65**) [e]	2.13
		[a]σ Cζ···Cε2	[c]σ*C3–H3(**7**) [e]	2.51
		[a]Cζ···Cε2	[c]σ*C5–H5(**44**) [e]	5.31
		[a], [b]LP(1)···Oη	[c]σ*O4–H4	2.80
		[a], [b]LP(2)···Oη	[c]σ*O4–H4	12.89
Tyrosine	90	[a], [b]LP(1)···Oη	[a]Cζ–Cε1	27.48
		[a], [b]LP(2)···Oη	[a]Cζ–Cε2	40.08
	−170[d]	[a], [b]LP(2)···Oη	[a]Cζ–Cε2	134.93

[a] Tyrosine.
[b] Oxygen lone pair (LP).
[c] Methyl β-D-glucopyranoside.
[d] Global minimum.
[e] Values in parenthesis are the corresponding orbital energy differences in kJ/mol. The energy difference = orbital energy of the complex – orbital energy of the monomer.

droxyl hydrogen of Tyr and the OMG hydroxyl O is ≈2.1 Å (Fig. 8a). At ϕ = 60°, the phenyl hydroxyl H has a severe steric clash with the H3 of the OMG OH group, as the separation distance is shorter, around 1.77 Å (Fig. 8b). Though the potential energy barrier height is the same for ϕ = −90° as 60°, the reason for the energy barrier is different in the −90° case. In this case, the barrier arises due to a perpendicular arrangement of the Tyr phenyl O–H bond vector with respect to Cγ–Cζ aromatic ring axis (Fig. 8c), and this bond is cis to Cα–Cβ bond, thereby losing its hyperconjugation interaction as observed for phenol derivatives.[33] Therefore, the stereoelectronic effect of the phenyl OH group is mainly participating in the stabilization of the OMG–Tyr complex, and it may have an influence on determining the orientation of the side chain torsions of Tyr residues in proteins.[34]

2.2. Implicit solvation of the complex

Dielectric continuum solvation calculations with integral equation formalism polarizable continuum model (IEFPCM[35–38]) using the default water values for the solvent radius and dielectric constant have been performed to understand the effect of solvation on the OMG–Tyr complex. The geometry of the OMG–Tyr model is considered from the minimum of gas phase PES obtained at MP2/6-311+G(d,p)//MP2/6-31G(d) levels of theory. The solvation Gibbs free energy of binding is obtained as the difference between the solvation Gibbs free energies of the complex and the monomers. This implicit solvation study resulted in a solvation Gibbs free energy of binding of $\Delta G_B \approx -11$ kJ/mol.

2.3. Computed IR and ^{1}H NMR Chemical shifts

Frequency calculations at the MP/6-31G(d) and M05-2X/6-311++G(d,p) levels have been utilized to analyze the bond stretching and direction IR frequency shift due to the C–H···π stacking upon the formation of the complex. Computed IR spectra corresponding to the C–H stretching modes are shown in Figure 9. Frequencies are scaled by 0.975 and 0.974 for MP/6-31G(d) and M05-2X/6-311++G(d,p) methods.[39] Blue shifts were calculated for the C1–H, C2–H, and C3–H stretching modes (44 cm^{-1}, 117 cm^{-1} and 48 cm^{-1}) from the IR spectrum of OMG to the OMG–TRY complex. However, on comparison of this direction of shift with M05-2X/6-311++G(d,p), the frequency shift of the C1–H mode is in the opposite direction (i.e., a red shift of ≈16 cm^{-1}). The C3–H and C5–H stretches are blue-shifted (57 and 37 cm^{-1}). Similar blue shifts were found by the modeling and experimental study on the C–H···π-bonded carbohydrate-aromatic complexes[40] and a small red shift has been observed for benzene complex.[41]

When the C–H bond vector of a hydrocarbon is close to an aromatic ring, the delocalized electrons of the aromatic ring change the local magnetic field of the H in the hydrocarbon, resulting in a significant upfield NMR chemical shift of the hydrocarbon H.[12] This resulting shift is called the deshielding effect and is caused by the ring current due to the benzene π electrons.[42] Hence, ^{1}H NMR spectroscopy was employed in experimental studies of intermolecular C–H···π interactions in various aromatic models and pyranose sugars.[18,21–24] As this NMR spectroscopic method is a potential tool to probe the presence of C–H···π interactions in aromatic amino acid–sugar complexes, shielding tensors using the gauge-including atomic orbital (GIAO)[43–47] method at the HF/6-31G(d,p)//MP2/6-31G(d,p), B3LYP/6-31G(d,p)//MP2/6-31G(d,p), and B3LYP/6-311+G(d,p)//MP2/6-31G(d) levels were computed. 2,2-Dimethyl-2-silapentane-5-sulfonate (DSS) was used as the reference compound.

The NMR characterization of the model system would provide strong evidence for the existence of the C–H···π interaction between OMG and Tyr if the calculated shifts can be observed. Table 5 lists the chemical shifts of the OMG protons on one face of the pyranose ring (H1, H2, H3, and H5). These results show the calculated changes due to the interaction with Tyr phenyl ring. In the case of the H3 and H4 protons, the shifts are downfield ($\Delta\delta$ = 0.12 and 0.02 ppm, respectively), indicating the least shield-

Table 4
Formation of Lewis and non-Lewis orbitals

Bond (A–B)	ED/energy (a.u.)	ED_A%	ED_B%	NBO	S%	P%	D
σ(C1–H1)	1.98	57.46	42.54	0.7580($sp^{2.88}d^{0.01}$) **C** + 0.6523 (s) **H**	25.76	74.06	0.18
σ(C3–H3)	1.97	58.79	41.21	0.7667($sp^{3.37}d^{0.01}$) **C** + 0.6420 (s) **H**	22.80	76.91	0.28
σ(C5–H5)	1.97	58.73	41.27	0.7664($sp^{3.22}$ $d^{0.01}$) **C** + 0.6424 (s) **H**	23.67	76.18	0.15
σ*(C1–H1)	0.039	42.54	57.46	0.6523($sp^{2.88}$ $d^{0.01}$) **C** − 0.7580 (s) **H**	25.76	74.06	0.18
σ*(C3–H3)	0.030	41.21	58.79	0.6420($sp^{3.37}$ $d^{0.01}$) **C** − 0.7667 (s) **H**	22.8	76.91	0.28
σ*(C5–H5)	0.027	41.27	58.73	0.6424($sp^{3.22}$ $d^{0.01}$) **C** − 0.7664 (s) **H**	23.67	76.18	0.15
σ(O–H)	1.98	75.69	24.31	0.8700($sp^{3.65}$ $d^{0.01}$) **O** + 0.4931(s) **H**	21.47	78.41	0.12
σ*(O–H)	0.01	24.31	**75.69**	0.4931($sp^{3.65}$ $d^{0.01}$) **O** − 0.8700 (s) **H**	21.47	78.41	0.12
LP1(O)	1.98			$sp^{1.11}$	47.39	52.58	0.02
LP2(O)	1.96			$sp^{1.83}$	1.59	98.38	0.03

Results are obtained for MP2/6-311+G(d,p) basis set. Here ED refers to electron density and LP refers to loan pair. Increased electron density of anti-bonding orbital of O–H bond has been highlighted to show the possible H-bond formation.

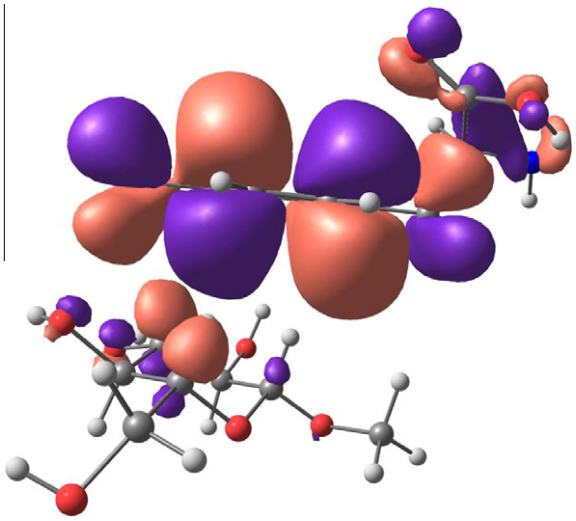

Figure 7. HOMO of the cellulose–binding module-cellulose model system obtained using NBO analysis with MP2/6-311+G(d,p) levels of theory. Complementary electron densities occur along C–H bonds of sugar and C–C_π of phenyl ring indicating the possible intermolecular C–H/π interactions.

ing for these ^{1}H atoms. Also, it should be noted here that the predicted chemical shift of H4 is almost zero. As the configurations of H3 and H2 are in the α and β faces of glucose, respectively, the shift should be upfield for H3 and downfield for H2. Hence, our computed NMR results suggest that the chemical shifts of the OMG–Tyr complex show the expected characteristic upfield shift for the H3 of C3.

3. Computational methods

Model building was done using Cerius[2] (Accelrys Inc.). All the quantum mechanical (QM) computations were carried out using GAUSSIAN 03.[48] Accurate modeling of the CH/π interaction energy and the appropriate interaction geometry is dependent on the choice of computational methods. Earlier studies on the selection of basis sets and the level of theory to explore this kind of weak interaction suggested the effectiveness of BHandHLYP functional.[24] Therefore, this method was considered with the cc-pVTZ basis set[49] along with the other methods[50–54] such as MP2/6-31G(d), MP2/6-31G(d,p), and MP2/6-31G(d)//MP2/6-311+G(d,p) for the present studies. A full geometry optimization was performed for the methyl β-D-glucopyranoside (OMG) and L-tyrosine (Tyr) complex (Fig. 1) before the scanning of PES was performed. To prevent the formation of an H-bond interaction by the C1 hydroxyl group of OMG with the tyrosine backbone, which would not be allowed with cellulose, the O1 atom was capped with a methyl group hence forming OMG model to mimic of cellulose linkage region.

Scans were performed for the complex using MP2/6-31G(d) and MP2/6-31G(d)//MP2/6-311+G(d,p) levels of theory to generate the relaxed potential energy surfaces (PES). To more precisely determine the interaction energy, the basis set superposition error (BSSE) correction was calculated using standard counterpoise correction method.[55] Comparison of the generated QM-based PES with that of the molecular mechanics (MM)-based PES was performed, and their corresponding interaction geometries were also compared. These MM calculations were performed using MM+ (HyperChem),[56] OPLS-AA, Amber94, MM2 (Macromodel, Schrodinger Inc.).

To address dispersive, intermolecular interactions, a meta-hybrid density functional called M05-2X has been developed.[30,57] As this method is computationally faster than the MP2 method, we also tested the M05-2X6-311++G(d,p) method for the presented system.

Gauge-independent atomic orbital (GIAO)[43–47] nuclear magnetic shielding tensors were computed for OMG–Tyr using the HF/6-311+G(d,p)//MP2/6-31G(d), B3LYP/6-311+G(d,p)//MP2/6-31G(d), and B3LYP/6-31G(d,p)//MP2/6-31G(d). 2,2-Dimethyl-2-silapentane-5-sulfonate (DSS) was used as reference molecule[18] to calculate the ^{1}H chemical shift of the OMG apolar protons. The shielding tensors for DSS were computed using HF/6-311+G(d,p)//B3LYP/6-31+G(d), B3LYP/6-311+G(d,p)//B3LYP/6-31+G(d), and B3LYP/6-31G(d,p)//B3LYP/6-31+G(d).

To compute the expected H-bond energy contributed by the Tyr phenyl hydroxyl group, conformational profiles were generated for both the isolated Tyr and the OMG–Tyr complex using the MP2/6-31G(d)//MP2/6-31G(d) and MP2/6-311+G(d,p)//MP2/6-31G(d) methods. The π-orbital of the aromatic ring plays a crucial role in the interaction with their counterpart C–H bond vectors from sugars.[13,58,59] Therefore, a minimum on the conformational energy surface was considered for NBO[32] analysis to explain the nature of orbital interaction between the C–H···π system, using the NBO 3.1 program implemented in GAUSSIAN 03. The free energies of interaction were further computed at the MP2/6-311+G(d,p)//MP2/6-31G(d) level using the self-consistent reaction field models using water as a solvent for the dielectric continuum. For this purpose, the integral equation formalism polarizable continuum model (IEFPCM) has been utilized.[35–38]

4. Conclusions

Investigations of the nature of forces between the aromatic ring in an amino acid, Tyr, and the monomer of cellulose polymer, OMG, have been made using molecular modeling, because this interaction plays an important role in crystalline and non-crystalline celluloses recognition by the CBM domain of cellulase enzymes. From

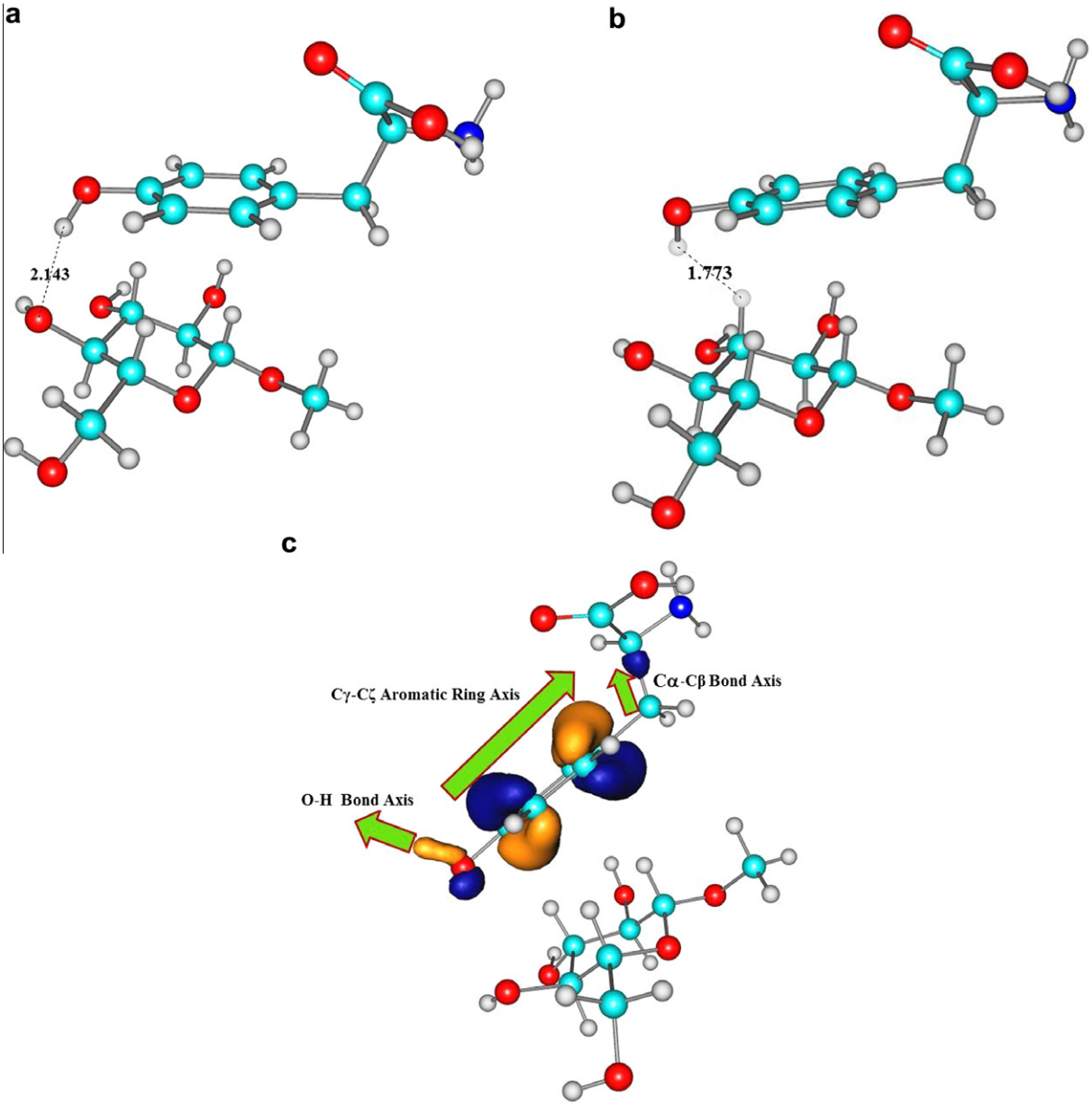

Figure 8. Non-bonded phenol hydroxyl H positions with respect to its neighbors at conformations (a) $\phi = 140$ and (b) $\phi = 60$ and (c) $\phi = -90$; here O–H bond vector lies perpendicular to Cγ–Cζ aromatic ring axis and hence bisects the ring plane along Cγ–Cζ axis.

these investigations, we surmised that the CH/π long-range dispersion forces are the secondary forces that supplement the dominant primary H-bond forces.

In the case of stacked configuration, the extensive overlap of OMG C–H bond vectors (e.g., C1–H1, C3–H3, and C5–H5) with the aromatic ring of Tyr is the origin of C–H···π stacking. The C3–H3 and C5–H5 vectors are present on either side of the phenyl hydroxyl H-bond channel. The interaction geometries of these vectors are shorter than that of the free end C1–H1. Therefore, formation of the H-bond between the Tyr phenyl hydroxyl group with the OMG O4 controls the stacking geometry of these C–H bond vectors. Co-existence of both the O–H···O-type classical H-bond and the C–H···π stacking indicates the cooperative nature of these two forces in the carbohydrate recognition process. The negative solvation Gibbs free energy ($\Delta G = -11$ kJ/mol, which does not include the configuration entropy contributions to ΔG from release of H_2O molecules), calculated for the OMG–Tyr complex, obtained with the MP2/6-311+G(d,p)//MP2/6-31G((d)) implicit solvation calculations, also favorably predicts the stabilization of this intermolecular stacking interaction in solution.

Acknowledgments

The research was funded by United States Department of Agriculture (USDA) through the Grant 'Improved Sustainable Cellulosic Materials Assembled Using Engineered Molecular Linkers' (that supported MNAM, JDK, JG, and JMC), by a USDA National Needs Graduate Fellowship—Grant No. 2007-38420-17782 (that supported HDW), and as part of The Center for LignoCellulose Structure and Formation, an Energy Frontier Research Center funded by the US Department of Energy, Office of Science, Office of Basic Energy Sciences under Award Number DE-SC0001090 (that supported JDK and JMC). Computational support was provided by the Research Computing and Cyberinfrastructure group at The

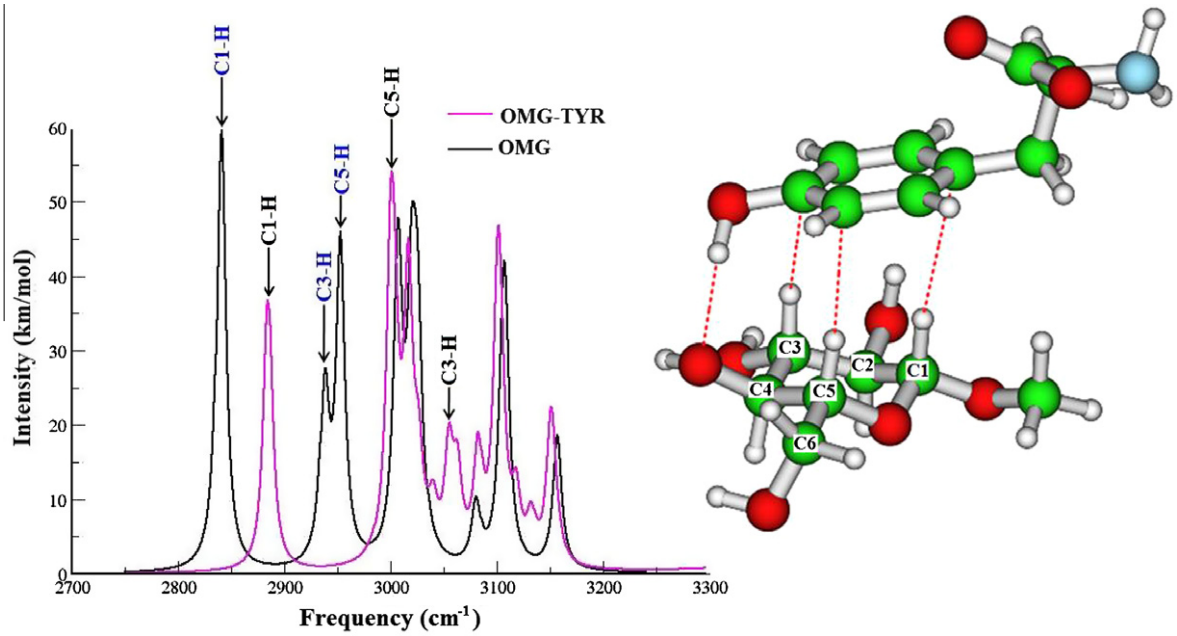

Figure 9. IR C–H spectra of *O*-methyl-β-D-Glc and the dimer calculated using the MP/6-31G(d) (scaled by 0.975). A lowest minimum structure is depicted alongside.

Table 5
Computed ^{1}H NMR chemical shifts of OMG and OMG–Tyr complex model

OMG	δ_0 (Glc) ppm			δ_c (Glc-Tyr) ppm			$\Delta\delta$ ($\delta_c - \delta_0$) ppm		
	HF/6-311+G(d,p)	B3LYP/6-31G(d,p)	B3LYP/6-311+G(d,p)	HF/6-311+G(d,p)	B3LYP/6-31G(d,p)	B3LYP/6-311+G(d,p)	HF/6-311+G(d,p)	B3LYP/6-31G(d,p)	B3LYP/6-311+G(d,p)
H1	**3.11**	**4.11**	**3.77**	**0.96**	**2.00**	**1.86**	**−2.15**	**−2.11**	−1.91
H2	2.94	2.92	3.04	2.62	2.72	2.77	−0.32	−0.2	−0.27
H3	2.58	3.25	2.96	2.71	3.39	3.35	0.13	0.14	0.39
H4	3.37	3.73	3.83	3.33	3.75	3.81	−0.04	0.02	−0.02
H5	2.41	3.11	2.89	2.34	2.84	2.96	−0.07	−0.27	0.07
O2H	−0.17	0.31	−0.59	0.00	−0.58	−0.31	0.17	0.27	0.28
O3H	2.50	2.37	2.35	2.37	1.88	2.20	−0.13	−0.49	−0.15
O4H	2.11	1.99	1.79	2.58	2.17	2.33	0.47	0.18	0.54

Shifts have been computed with reference to DSS. Calculations were done using HF/6-311+G(d,p)//MP2/6-31G(d), B3LYP/6-31G(d,p)//MP2/6-31G(d) and B3LYP/6-311+G(d,p)//MP2/6-31G(d) methods.

Pennsylvania State University. The authors would like to thank Professor Kristin Bartik of Université Libre de Bruxelles for her invaluable discussions regarding thermodynamics and NMR spectra.

Supplementary data

Supplementary data associated with this article can be found, in the online version, at doi:10.1016/j.carres.2010.05.021.

References

1. Tilbeurgh, H. V.; Tomme, P.; Claeyssens, M.; Bikhabai, R.; Pettersson, G. *FEBS Lett.* **1986**, *204*, 223–227.
2. Tomme, P.; Tilbeurgh, H. V.; Pettersson, G.; Damme, J. V.; Vandekerchove, J.; Knowles, J.; Teeri, T. T.; Claeyssens, M. *Eur. J. Biochem.* **1988**, *170*, 575–581.
3. Gill, J.; Rixon, J. E.; Bolam, D. N.; McQueen-Mason, S.; Simpson, P. J.; Williamson, M. P.; Hazlewood, G. P.; Gilbert, H. J. *Biochem. J.* **1999**, *342*, 473–480.
4. Cantarel, B. L.; Coutinho, P. M.; Rancurel, C.; Bernard, T.; Lombard, V.; Henrissat, B. *Nucleic Acids Res.* **2008**, *37*, D233–D238.
5. Boraston, B. A.; Bolam, D. N.; Gilbert, H. J.; Davies, G. J. *Biochem. J.* **2004**, *382*, 769–781.
6. Pettersson, G.; Linder, M.; Reinikainen, T.; Drakenberg, T.; Mattinen, M. L.; Annila, A.; Kontteli, M.; Lindeberg, G.; Stahlberg, J. *Protein Sci.* **1995**, *4*, 1056–1064.
7. McLean, B. W.; Bray, M. R.; Boraston, A. B.; Gilkes, N. R.; Haynes, C. A.; Kilburn, D. G. *Protein Eng.* **2000**, *13*, 801–809.
8. Xie, H.; Gilbert, H. J.; Charnock, S. J.; Dias, F. M.; Ferreira, L. M.; Bolam, D. N. *Biochemistry* **2001**, *40*, 9167–9176.
9. Xiao, Z.; Gao, P.; Qu, Y.; Wang, T. *Biotechnol. Lett.* **2001**, *23*, 711–715.
10. Rao, V. S. R.; Qasba, P. K.; Balaji, P. V.; Chandrasekaran, R. *Conformation of Carbohydrates*; Harwood Academic: The Netherlands, 1998.
11. Imberty, A.; Gautier, C.; Lescar, J.; Perez, S.; Wyns, L.; Loris, R. *J. Biol. Chem.* **2000**, *275*, 17541–17548.
12. Elgavish, S.; Shaanan, B. *TIBS* **1997**, *22*, 462–467.
13. Nishio, M.; Hirota, M.; Umezawa, Y. In *The CH/π Interaction: Evidence, Nature, and Consequences, Methods in Stereochemical Analysis*; Marchand, A. P., Ed.; Wiley-VCH: New York, 1998.
14. Tsuzuki, S.; Honda, K.; Uchimaru, T.; Mikami, M.; Tanabe, K. *J. Am. Chem. Soc.* **2000**, *122*, 3746–3753.
15. Tsuzuki, S.; Honda, K.; Uchimaru, T.; Mikami, M.; Fujii, A. *J. Phys. Chem. A* **2006**, *110*, 10163–10168.
16. Sharma, R.; McNamara, J. P.; Raju, R. K.; Vincent, M. A.; Hillier, I. H.; Morgado, C. A. *Phys. Chem. Chem. Phys.* **2008**, *10*, 2767–2774.
17. Unezawa, Y.; Tsuboyama, S.; Honda, K.; Uzawa, J.; Nishio, M. *Bull. Chem. Soc. Jap.* **1998**, *71*, 1207–1213.
18. Vandenbussche, S.; Diaz, D.; Fernández-Alonso, M. D. C.; Pan, W.; Vincent, S. P.; Cuevas, G.; Canada, F. J.; Jimenez-Barbero, J.; Bartik, K. *Chem. Eur. J.* **2008**, *14*, 7570–7578.
19. Spiwok, V.; Lipovová, P.; Skálová, T.; Buchtelová, E.; Hašekb, J.; Králová, B. *Carbohydr. Res.* **2004**, *339*, 2275–2280.
20. Nishiyama, Y.; Langan, P.; Chanzy, H. *J. Am. Chem. Soc.* **2002**, *124*, 9074–9082.
21. *NMR Spectroscopy of Glycoconjugates*; Jimenez-Barbero, J., Peter, T., Eds.; Wiley-VCH: Weinheim, Germany, 2003.

22. Vliegenthart, F. G. J. *NMR Spectroscopy and Computer Modeling of Carbohydrates: Recent Advances*; Vliegenthart, F. G. J.; Woods, R. J., Eds.; ACS Symposium Series, 2006, pp 1–39.
23. Poveda, A.; Jiménez-Barbero, J. *Chem. Soc. Rev.* **1998**, *27*, 133–144.
24. Fernández-Alonso, M. D. C.; Cañada, F. J.; Jiménez-Barbero, J.; Cuevas, G. *J. Am. Chem. Soc.* **2005**, *127*, 7379–7386.
25. Csontos, J.; Palermo, N. Y.; Murphy, R. F.; Lovas, S. *J. Comput. Chem.* **2008**, *29*, 1344–1352.
26. Vondrášek, J.; Bendová, L.; Klusák, V.; Hobza, P. *J. Am. Chem. Soc.* **2005**, *127*, 2615–2619.
27. Jurečka, P.; Šponer, J.; Černy, J.; Hobza, P. *Phys. Chem. Chem. Phys.* **2006**, *8*, 1985–1993.
28. Berman, H. M.; Westbrook, J.; Feng, Z.; Gilliland, G.; Bhat, T. N.; Weissig, H.; Shindyalov, I. N.; Bourne, P. E. *Nucleic Acids Res.* **2000**, *28*, 235–242.
29. Lütteke, T.; Frank, M.; von der Lieth, C. W. *Nucleic Acids Res.* **2005**, *33*, D242–D246.
30. Zhao, Y.; Truhlar, D. G. *Acc. Chem. Res.* **2008**, *41*, 157–167.
31. Spiwok, V.; Lipovová, P.; Skálová, T.; Vondráčková, E.; Dohnálek, J.; Hašek, J.; Králová, B. *J. Comput. Aided Mol. Des.* **2006**, *19*, 887–901.
32. Reed, A. E.; Curtiss, L. A.; Weinhold, F. *Chem. Rev.* **1988**, *88*, 899–926.
33. Richardson, P. R.; Chapman, M. A.; Wilson, D. C.; Bates, S. P.; Jones, A. C. *Phys. Chem. Chem. Phys.* **2002**, *4*, 4910–4915.
34. Langella, E.; Rega, N.; Improta, R.; Crescenzi, O.; Barone, V. *J. Comput. Chem.* **2002**, *23*, 650–661.
35. Cances, E.; Mennucci, B.; Tomasi, J. *J. Chem. Phys.* **1997**, *107*, 3032–3041.
36. Mennucci, B.; Cances, E.; Tomasi, J. *J. Phys. Chem. B* **1997**, *101*, 10506–10517.
37. Mennucci, B.; Tomasi, J. *J. Chem. Phys.* **1997**, *106*, 5151–5158.
38. Tomasi, J.; Mennucci, B.; Cances, E. *J. Mol. Struct.: THEOCHEM* **1999**, *464*, 211–226.
39. http://comp.chem.umn.edu/truhlar/freq_scale.htm.
40. Su, Z.; Cocinero, E. J.; Stanca-Kaposta, E. C.; Davis, B. G.; Simons, J. P. *Chem. Phys. Lett.* **2009**, *471*, 17–21.
41. Dinadayalane, T. C.; Leszczynski, J. *J. Chem. Phys.* **2009**, *130*, 081101–081104.
42. Ran, J.; Wong, M. W. *J. Phys. Chem. A* **2006**, *110*, 9702–9709.
43. London, F. *J. Phys. Radium, Paris* **1937**, *8*, 397–409.
44. McWeeny, R. *Phys. Rev.* **1962**, *126*, 1028–1034.
45. Ditchfield, R. *Mol. Phys.* **1974**, *27*, 789–807.
46. Dodds, J. L.; McWeeny, R.; Sadlej, A. J. *Mol. Phys.* **1980**, *41*, 1419–1430.
47. Wolinski, K.; Hilton, J. F.; Pulay, P. *J. Am. Chem. Soc.* **1990**, *112*, 8251–8260.
48. GAUSSIAN 03, Revision C.02, Frisch, M. J.; Trucks, G. W.; Schlegel, H. B.; Scuseria, G. E.; Robb, M. A.; Cheeseman, J. R.; Montgomery, J. A., Jr.; Vreven, T.; Kudin, K. N.; Burant, J. C.; Millam, J. M.; Iyengar, S. S.; Tomasi, J.; Barone, V.; Mennucci, B.; Cossi, M.; Scalmani, G.; Rega, N.; Petersson, G. A.; Nakatsuji, H.; Hada, M.; Ehara, M.; Toyota, K.; Fukuda, R.; Hasegawa, J.; Ishida, M.; Nakajima, T.; Honda, Y.; Kitao, O.; Nakai, H.; Klene, M.; Li, X.; Knox, J. E.; Hratchian, H. P.; Cross, J. B.; Bakken, V.; Adamo, C.; Jaramillo, J.; Gomperts, R.; Stratmann, R. E.; Yazyev, O.; Austin, A. J.; Cammi, R.; Pomelli, C.; Ochterski, J. W.; Ayala, P. Y.; Morokuma, K.; Voth, G. A.; Salvador, P.; Dannenberg, J. J.; Zakrzewski, V. G.; Dapprich, S.; Daniels, A. D.; Strain, M. C.; Farkas, O.; Malick, D. K.; Rabuck, A. D.; Raghavachari, K.; Foresman, J. B.; Ortiz, J. V.; Cui, Q.; Baboul, A. G.; Clifford, S.; Cioslowski, J.; Stefanov, B. B.; Liu, G.; Liashenko, A.; Piskorz, P.; Komaromi, I.; Martin, R. L.; Fox, D. J.; Keith, T.; Al-Laham, M. A.; Peng, C. Y.; Nanayakkara, A.; Challacombe, M.; Gill, P. M. W.; Johnson, B.; Chen, W.; Wong, M. W.; Gonzalez, C.; Pople, J. A.; Gaussian Inc., Wallingford CT, 2004.
49. Kendall, R. A.; Dunning, T. H., Jr.; Harrison, R. J. *J. Chem. Phys.* **1992**, *96*, 6796–6806.
50. Head-Gordon, M.; Pople, J. A.; Frisch, M. *J. Chem. Phys. Lett.* **1988**, *153*, 503–506.
51. Frisch, M. J.; Head-Gordon, M.; Pople, J. A. *Chem. Phys. Lett.* **1990**, *166*, 275–280.
52. Frisch, M. J.; Head-Gordon, M.; Pople, J. A. *Chem. Phys. Lett.* **1990**, *166*, 281–289.
53. Head-Gordon, M.; Head-Gordon, T. *Chem. Phys. Lett.* **1994**, *220*, 122–128.
54. Saebo, S.; Almlof, J. *Chem. Phys. Lett.* **1989**, *154*, 83–89.
55. Boys, S. F.; Bernardi, F. *Mol. Phys.* **1970**, *19*, 553–566.
56. Hyperchem, Release 7.0, Hypercube Inc., 1115 NW 4th Street, Gainesville, FL 32601, USA.
57. Zhao, Y.; Schultz, N. E.; Truhlar, D. G. *J. Chem. Theory Comput.* **2006**, *2*, 364–382.
58. Dougherty, D. A. *Science* **1996**, *271*, 163–168.
59. Laughrey, Z. R.; Kiehna, S. E.; Riemen, A. J.; Waters, M. L. *J. Am. Chem. Soc.* **2008**, *130*, 14625–14633.